Polymer 49 (2008) 2568–2577

Contents lists available at ScienceDirect

Polymer

journal homepage: www.elsevier.com/locate/polymer

Interplay between crystallization behaviors and extensional deformation of isotactic polypropylene and its blend with poly(ethylene-*co*-octene)

Yongyan Pang [a,b], Xia Dong [a,*], Xiuqin Zhang [a], Kaipeng Liu [c], Erqiang Chen [c], Charles C. Han [a], Dujin Wang [a,*]

[a] *Beijing National Laboratory for Molecular Sciences, CAS Key Laboratory of Engineering Plastics, State Key Laboratory of Polymer Physics and Chemistry, Institute of Chemistry, Chinese Academy of Sciences, Beijing 100190, China*
[b] *Graduate School of Chinese Academy of Sciences, Beijing 100190, China*
[c] *Beijing National Laboratory for Molecular Sciences, Department of Polymer Science and Engineering and the Key Laboratory of Polymer Chemistry and Physics of Ministry of Education, College of Chemistry and Molecular Engineering, Peking University, Beijing 100871, China*

ARTICLE INFO

Article history:
Received 10 January 2008
Received in revised form 25 March 2008
Accepted 29 March 2008
Available online 4 April 2008

Keywords:
Isotactic polypropylene/poly(ethylene-*co*-octene) blend
Crystallization behavior
Extensional deformation

ABSTRACT

Comparison investigation of the interaction between crystallization behaviors and extensional deformation of both isotactic polypropylene (iPP) and its blend with poly(ethylene-*co*-octene) (iPP/PEOc) was carried out in this study. The samples of iPP and the iPP/PEOc (80/20, wt.%) blend were prepared by changing the cooling rate during nonisothermal crystallization. Tensile testing showed that with the decrease of cooling rate, the progressive destruction of ductility of the two samples was resulted from the more perfect crystallites formed in the cooling process. The influence of cooling rate on the tensile properties is more prominent for pure iPP than for the iPP/PEOc blend. The crystalline structure was proven to be partially destroyed under the extensional deformation, and such crystalline structure destruction was in close association with the deformation of the specimens. The oriented noncrystalline molecular chains could easily be reorganized into more perfect crystals in postheating runs. The original crystalline structure has been found, to some extent, to determine the extensional deformation and the final crystallization behavior.

1. Introduction

Isotactic polypropylene (iPP) has extensive applications such as fibers, tubes, films, transparent products, etc, by virtue of its outstanding merits including chemical resistance, electrical resistance, low density and relatively low cost, and so on. The poor impact toughness, particularly at low temperature, however, limits the wide usage of iPP as a general plastic [1–5]. Since 1990s, the copolymer of ethylene and octene (PEOc) has been invented as an excellent iPP impact modifier following EPR, EPDM and SBS, due to its easy processing characteristics and good dispersion in the iPP matrix [6,7]. The iPP/PEOc blend has been investigated from different aspects such as crystallization and melting behavior, mechanical properties, morphological evolution, rheological properties, etc [1–4,8–12]. According to previous studies, the addition of PEOc in iPP can depress the total degree of crystallinity, thus resulting in the decrease of the tensile properties of the blends. The elongation at break, however, can only be improved within a limited concentration of elastomer phase [1,3,9].

The investigation on the mechanical properties of polyolefins and their blends has been attracting researchers' attention for several decades [13–18], which are the guidelines for product applications from industrial points of view. Numerous studies have been carried out in this area concerning the molding methodology [19,20], deformation mechanism [21,22], plastic deformation in plane-strain compression [23–27], as well as tensile properties of crystalline polymers [17,18,28,29]. The stress–strain curves of polyolefins and their blends were found strongly dependent on the molecular parameters, supermolecular structures and testing conditions. The extensional deformation of such semi-crystalline polymers is characterized by some processes such as elastic deformation, yielding, strain softening, necking, and strain hardening. The deformation process always involves structure changes like the dislocation and distortion of crystals, sliding and slipping, twisting and dissociation of lamellae, unfolding of molecular chains, cavitation and fibrillation, and so on [13–15]. Although many theories concerning the deformation mechanisms have been proposed, some structural deformation in polyolefin materials still remains far from being well understood [17,18].

Concerning the factors affecting the mechanical properties of iPP, it is believed that the molding methodology, the testing conditions such as temperature and tensile speed, crystalline structure,

* Corresponding authors. Tel.: +86 10 82618533; fax: +86 10 62521519.
E-mail addresses: xiadong@iccas.ac.cn (X. Dong), djwang@iccas.ac.cn (D. Wang).

0032-3861/$ – see front matter © 2008 Elsevier Ltd. All rights reserved.
doi:10.1016/j.polymer.2008.03.050

and the introduction of copolymers all govern the ultimate performances [10,11,13,19,28]. The mechanical properties of the iPP/PEOc blends at different tensile speeds have been investigated to elucidate the brittle–ductile transition [10]. The testing temperature was found to show an opposite effect on influencing the mechanical properties as tensile speed does, i.e., the tensile properties have the same variation trend under higher temperature as those applied with slower tensile speed [10,13]. However, the effect of crystalline morphology on the mechanical properties of the iPP/PEOc blends has been seldom reported. According to the previous studies [11,13,17,19,28,30], the crystallinity and morphology contribute a lot to the final performance of semi-crystalline polymers and their blends.

In a previous paper, we investigated the relationship between the morphology evolution and corresponding mechanical properties, and the crystallization procedure was roughly proven to play an important role on influencing the mechanical properties [11]. In the present work, the effect of crystallization condition and crystalline morphology on tensile properties of pure iPP and the iPP/PEOc (80/20) blend has been studied, and the influence of the elastomer phase on the extensional deformation of the iPP/PEOc blend has been paid much attention. Moreover, the crystallization of undeformed and deformed regions is compared, in order to reveal the effect of extensional deformation on the crystallization behavior of iPP and the PEOc components. At last, a schematic illustration for the interplay between the crystallization behavior and extensional deformation of iPP and the iPP/PEOc blend will be proposed to elucidate the deformation mechanism.

2. Experimental

2.1. Materials

Isotactic polypropylene resin (iPP, 1300) ($M_w = 4.1 \times 10^5$, $M_w/M_n = 4$, MFI = 1.5 g/10 min) was provided by Beijing Yanshan Petrochemical Co. Ltd. (China). Engage 8150 ($M_w = 1.5 \times 10^5$, $M_w/M_n = 2$, MFI = 0.5 g/10 min), a metallocene catalyzed copolymer of ethylene and 1-octene (PEOc) with 30.6 wt.% of comonomer, was purchased from DuPont–Dow Elastomers. The molecular weight and molecular weight distribution were measured by GPC. The comonomer content of PEOc was calculated according to ^{13}C NMR spectrum.

2.2. Preparation of iPP/PEOc blend

The iPP/PEOc blend containing 80 wt.% iPP and 20 wt.% PEOc was prepared using a TSE-30A co-rotating twin screw extruder with an L/D of 40. The temperatures from feed to die zones were set at 180, 190, 200, 220, 220, 220, 220, 200, 190 and 180 °C, respectively, and the screw speed was 100 rpm. The extrudates were chopped into pellets for the following experiments. Sample blending was performed twice to obtain better dispersion effect. For comparison, pure iPP underwent the same treatment in the extruder as that of the iPP/PEOc blend.

2.3. Optical microscopic observations

The crystalline morphology of iPP and the iPP/PEOc (80/20) blend obtained with different cooling rates was studied with an Olympus BX51 polarized optical microscope (POM) connected with a Linkam THMS600 hot stage under nitrogen atmosphere. The cooling rate was controlled with the aid of liquid nitrogen. The samples used for POM observation were films with thickness of ca. 30 μm, which were prepared with a homemade compression molder. The films were first melted at 200 °C and then cooled to 35 °C at different cooling rates, i.e., 2 °C/min, 5 °C/min, 15 °C/min and quenching, identical with the preparation processes of mechanical samples described below. The polarized optical micrographs were taken after the samples reached 35 °C.

2.4. Tensile test

2.4.1. Sample preparation

The samples for tensile tests were prepared at a series of cooling rates. The pellets of iPP or the iPP/PEOc (80/20) blend were preheated at 200 °C on an LP-S-50 compression molder for 5 min (t_h), pressed for 2 min (t_p) with the pressure of 5 MPa, and then cooled to 35 °C at various cooling rates, i.e., 15 °C/min, 5 °C/min or 2 °C/min under pressure. An exceptional one, denoted as quenched sample, was directly transferred to a TDM-50-2 compression molder with the temperature set at 35 °C and pressure at 5 MPa after the preheating and compressing in the LP-S-50 compression molder. All the samples were kept at 35 °C for 5 min. The illustration of the preparation process of the primary sheets is shown in Fig. 1.

2.4.2. Extensional deformation tests

The tensile bars were cut out from the primary sheets with an RP/PCP pneumatic serving machine according to GB13022-91 with the rectangular dimensions of $25 \times 6 \times 1$ mm^3. They were held in an LRH-250A cultivation cabinet with constant temperature (23 °C) and humidity (50%) for 48 h before testing.

The uniaxial tensile deformation was carried out on an Instron 3365 Universal mechanical testing machine at room temperature, at a crosshead speed of 50 mm/min. The extensional deformation was imposed until the tensile bars were broken at the longest strain. The stress–strain curves were recorded and the tensile bars were kept for DSC and XRD measurements. All the mechanical property data presented were the averages of five samples.

2.5. Melting and crystallization characterization

2.5.1. DSC measurements

A Perkin–Elmer differential scanning calorimeter (model DSC7) was applied to investigate the melting behavior of the samples prepared at various cooling rates (2 °C/min, 5 °C/min, 15 °C/min, and quenching). The undeformed samples were selected from the remaining part of iPP or the iPP/PEOc blend sheets after the tensile bars were cut out. The deformed regions were taken from the deformed part of the tensile samples. The heating scans were performed at a temperature range from 0 °C to 200 °C at a heating rate of 10 °C/min under nitrogen atmosphere. Melting temperatures and fusion enthalpy were determined from the heating runs to estimate the perfection of the crystals. The instrument was calibrated with standard indium.

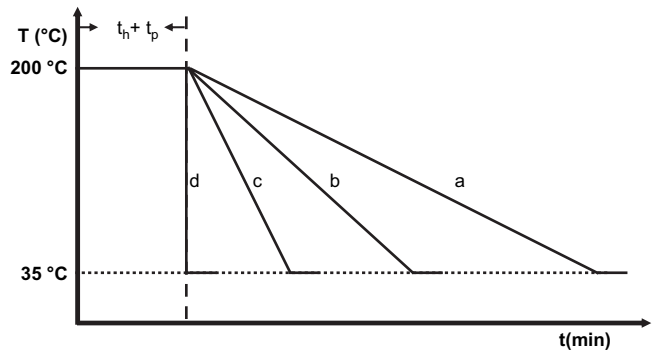

Fig. 1. Sample preparation processes for iPP and the iPP/PEOc blend at different cooling rates: (a) 2 °C/min; (b) 5 °C/min; (c) 15 °C/min, and (d) quenched.

2.5.2. X-ray diffraction

Wide angle X-ray diffraction measurement was carried out using a Bruker D8 Discover diffractometer equipped with GADDS (spatial resolution: $105 \times 105\ \mu m^2$/pixel) as a 2D detector in transmission mode. The X-ray sources (Cu Kα, $\lambda = 1.54$ Å) were provided by 3 kW ceramic tubes, and the diffraction peak positions were calibrated with silicon powder ($2\theta > 15^\circ$) and silver behenate ($2\theta < 10^\circ$). The two-dimensional (2D) diffraction patterns were investigated for both the undeformed and deformed regions at room temperature with the exposure time of 300 s. The point-focused X-ray beam of 0.2 mm in diameter was aligned perpendicular to the mechanical stretching direction. The background scattering was recorded and subtracted from the sample patterns.

3. Results and discussion

3.1. Morphology investigation

The POM images presented in Fig. 2 show the crystalline morphology of iPP and the iPP/PEOc (80/20) blend after cooled to 35 °C at different cooling rates. It is clear that as the cooling rate increases, the crystal size decreases from ca. 100 μm to 10 μm, with the spherulitic boundaries changing from sharp to diffuse. The crystals of the iPP/PEOc (80/20) blend are more defective than those of pure iPP, because the introduction of PEOc component hinders the crystallization of iPP, as previously reported in the iPP catalloys [31]. Comparing the spherulitic morphologies of pure iPP and the iPP/PEOc (80/20) blend cooled at 2 °C/min, PEOc component lies at the boundary of the iPP spherulites, or exhibits as dark points of trapped PEOc inclusions in the iPP spherulites. However, due to smaller crystal sizes, the morphological difference is not prominent for the faster cooling samples of iPP and the iPP/PEOc blend. According to the previous studies [32,33], the PEOc domains are dispersed in the iPP matrix, so when iPP crystallizes at given conditions, the PEOc molecules are thought to be excluded into the interspherulitic regions or between lamellae stacks of the iPP spherulite. In addition, it has been reported that the iPP spherulites can grow around the PEOc droplets and trap the elastomer phase in crystalline domains [12], therefore, the PEOc component in the present work can lie as trapped inclusions in the iPP spherulites. Considering its existing location, PEOc may on one hand affect the perfection of the iPP crystals, and on the other hand add to the amorphous connections between the iPP crystals. So, it is reasonable to imagine that the incorporation of PEOc component may increase the ductility and hence change the mechanical properties of the specimens.

Table 1
Tensile properties of iPP and the iPP/PEOc (80/20) blend prepared at different cooling rates

Cooling rate (°C/min)	Yield strength (MPa)		Break strength (MPa)		Elongation at break (%)	
	iPP	iPP/PEOc	iPP	iPP/PEOc	iPP	iPP/PEOc
Quenched	35.2 ± 0.7	23.6 ± 0.1	25.7 ± 3.9	39.8 ± 3.8	690 ± 20	850 ± 40
15	36.0 ± 0.0	23.7 ± 0.2	22.5 ± 2.5	37.9 ± 3.4	250 ± 20	800 ± 60
5	35.7 ± 0.2	23.3 ± 0.4	23.1 ± 1.9	33.8 ± 2.7	160 ± 40	730 ± 50
2	36.1 ± 0.5	23.2 ± 0.3	30.3 ± 8.2	28.3 ± 5.1	20 ± 10	650 ± 30

3.2. Tensile property analysis

The influence of cooling rate on tensile properties is shown in Fig. 3 and Table 1. The elongation at break decreases with decreasing the cooling rates for both iPP and the iPP/PEOc (80/20) blend, indicating that the gradual perfection of crystals during the nonisothermal crystallization results in breakage of ductility. The break strength first decreases and then increases for iPP but always decreases for the blend, which might be attributed to the different breaking manners. The addition of elastic component in the blend facilitates the larger elongation in ductile fracture manner, and the phenomenon of strain hardening is remarkable for all the specimens of the blend, displaying a depressed trend with the decrease of cooling rate. However, strain hardening behaves fairly weak for the quenched iPP specimen. The occurrence of strain hardening is accompanied with longer extension and higher stress. As a result, the elongation at break and the break strength decrease as the cooling rate decreases for the iPP/PEOc (80/20) blend. Whereas, for pure iPP, the quenched specimen exhibits larger break strength, while all the other samples were fractured in the necking zones. As a result, the break strength increases with decreasing cooling rate. According to the previous reports, crystallinity and crystalline morphology exert important influence on the yield strength, which increases linearly [13,17] or exponentially [30] with crystallinity. In this study, however, the yield strength of the two samples shows nearly no dependence on the cooling rate. This may be attributed to the fact that the crystallinity does not change significantly with cooling rate (Table 2). Right after yielding, there is a sharp drop in load for iPP, termed as strain softening, which is associated with the dislocation of the original crystals. Compared with iPP, the yield strength of the iPP/PEOc (80/20) blend is much lower and the yielding process is not so sharp (Fig. 3b), which agrees well with the

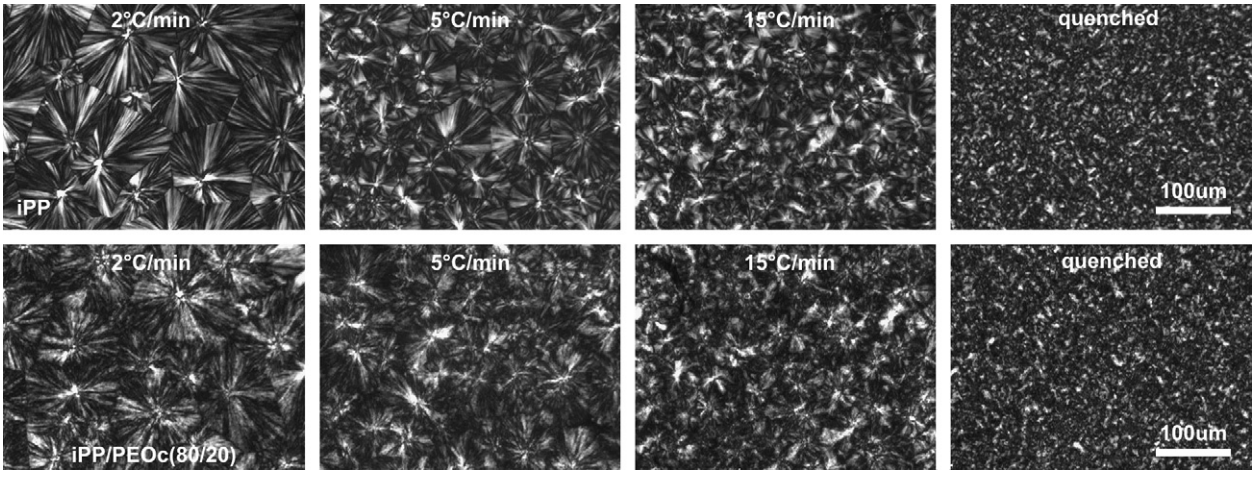

Fig. 2. POM morphologies of iPP and the iPP/PEOc (80/20) blend after melting at 200 °C and then cooled down to 35 °C at various cooling rates.

Table 2
Melting behavior of undeformed regions of iPP prepared at different cooling rates

Cooling rate (°C/min)	Quenched	15	5	2
Onset (°C)	155.0	157.4	157.7	159.6
T_m (°C)	162.5	164.7	165.0	165.6
ΔH (J/g)	94.6	96.7	100.1	104.7
X_c^{iPP}	45.3	46.3	47.9	50.1

previous reports that the yielding becomes diffuse with the addition of copolymers [10,32,34]. The stress drop of the iPP/PEOc (80/20) blend after yielding shows the same variation trend as that of iPP with the decrease of cooling rate, but the load decreases less, which is thought to be associated with the imperfection of the iPP crystals and higher ability of dislocating themselves in the blend. Moreover, the extensional flow becomes unstable with the addition of the PEOc component, exhibiting abrupt stress increase and decrease after yielding, which has not been well understood up to date. Nevertheless, it is unambiguously showed in Fig. 3 and Table 1 that, the influence of cooing rate on tensile properties is more obvious for pure iPP than for the iPP/PEOc (80/20) blend, and the origin will be discussed later on.

3.3. Interaction between crystallization behaviors and extensional deformation

The melting behavior of the undeformed regions in pure iPP and the iPP/PEOc blend was first investigated to reveal the crystallization characteristics of iPP under various conditions and consequently to make it clear how the crystallization interacts with extensional deformation.

The influence of cooling rate on the crystallization behavior of undeformed iPP is shown in Fig. 4a. As the cooling rate decreases, the melting peaks shift to higher temperatures, and the normalized melting enthalpy increases correspondingly (Table 2). All these results indicate that the undeformed samples prepared at slower cooling rates are composed of crystals with thicker lamellae, while those prepared at faster cooling rates contain more defective crystals with thinner lamellae. Combining the investigations of mechanical properties, it is obvious that the samples comprised of crystals with thicker lamellae exhibit smaller elongation at break, while the crystals comprising of thinner lamellae manifest longer elongation. It is believed that crystals of larger sizes and higher perfection have less ability to rearrange themselves under stretching and therefore cannot sustain larger extensional deformation, consistent with the previous reports [11,17,34]. The normalized percentage of crystallinity of iPP was roughly calculated according to Eq. (1) [1,3]:

$$X_c = \frac{\Delta H_f^{obs}}{\Delta H_f^o}\frac{1}{W} \times 100\% \quad (1)$$

where ΔH_f^o is taken as 209 J/g for 100% crystalline iPP and W is the weight fraction of iPP, which is 100% for pure iPP. As the melting enthalpy increases with the decrease of cooling rate, the crystallinity degree increases (Table 2), and accordingly, the amorphous populations decrease. The amorphous region at the iPP spherulites boundaries can act as the interspherulitic connections. From the observation of POM images, the boundaries of the iPP spherulites changes from dull to sharp as the cooling rate decreases. It is

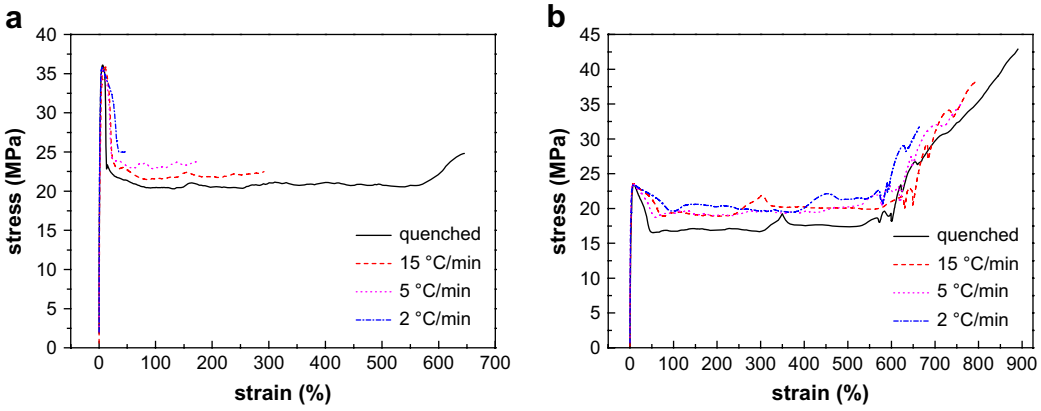

Fig. 3. Stress–strain curves for iPP (a) and the iPP/PEOc (80/20) blend (b) prepared at different cooling rates.

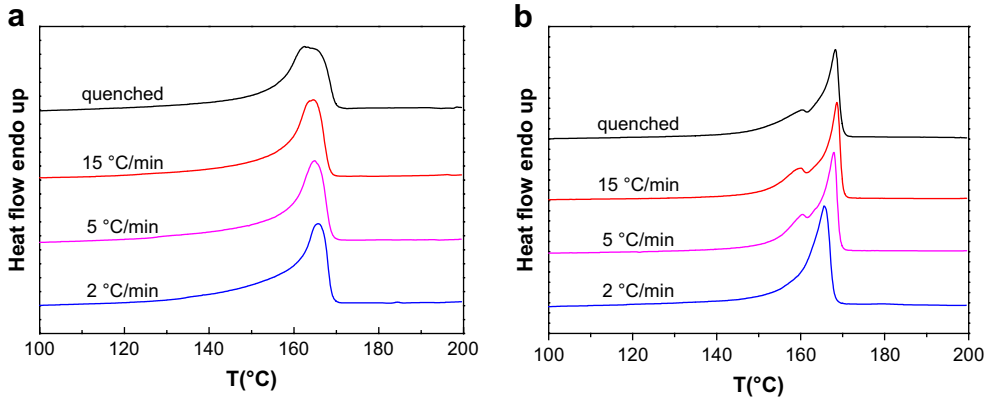

Fig. 4. DSC heating scans (10 °C/min) of the iPP samples prepared at different cooling rates: (a) undeformed regions and (b) deformed regions.

Table 3
Melting behavior of deformed regions of iPP prepared at different cooling rates

Cooling rate (°C/min)	Quenched	15	5	2
Onset (°C)	164.2	165.0	163.6	160.2
T_{m1} (°C)	160.5	160.3	160.5	–
T_{m2} (°C)	168.3	168.6	168.0	165.6
ΔH (J/g)	98.3	100.9	106.6	107.4

acceptable that if neighboring spherulites share sharper boundary, extensibility will be worse, for voids will be formed at the sharper boundary during stretching.

The melting behavior of the deformed region was also investigated to gain deep insight into the effect of the uniaxially extensional deformation on the crystallization behavior of tensile samples.

The melting process displays that there are dual melting peaks for the deformed iPP crystallized at the employed cooling rates (Fig. 4b and Table 3) except that crystallized at 2 °C/min. The lower melting peak of the deformed region moves to lower temperature compared with that of undeformed region. Correspondingly, the higher melting peak of the deformed region moves to higher temperature after stretched, which may be due to two possibilities. One is that some molecular chains or segments are preferentially oriented along stretching direction and recrystallized during stretching, known as strain-induced crystallization [35–37]; the other is that the molecular chains or segments are rearranged into crystals of higher perfection during postheating process. According to the WAXD results, the latter is more probable, which will be discussed later on.

Fig. 5a_1 and a_2 shows the influence of cooling rates on the crystallization behavior of iPP and the PEOc component in the undeformed iPP/PEOc (80/20) blend. Compared with pure iPP, similar crystallization results were obtained for the iPP component in the blend, including the melting temperature and melting enthalpy. The appearance of the broad weak dual melting peaks of the PEOc component reveals its somewhat crystallization behavior, which has been reported previously [4–7,38,39]. The cooling rate does not show unambiguous influence on the crystallization behavior of PEOc component, which might be attributed to its much weaker crystallization ability. Associating with the mechanical properties of the iPP/PEOc (80/20) blend, although the elongation at break and the break strength decrease with the decreasing of cooling rate, these changes are not as prominent as those of pure iPP. One reason is that the crystals of the iPP component in the iPP/PEOc (80/20) blend are less perfect than those of pure iPP, thus are easier to dislocate and rearrange themselves under stretching, and consequently are propitious to tensile deformation. Another reason is that the amorphous PEOc component existing between the iPP spherulites or lamellae stacks plays the role of interspherulitic connections. As a result, the elastomer phase makes the blend sustain longer extension and facilitates the occurrence of strain hardening, resulting in higher break strength. Generally speaking, the addition of PEOc component in the blend facilitates the applied extensional deformation and contributes to the elongation of tensile bars. Moreover, the presence of PEOc component in the blend retards the response of mechanical properties on the cooling rate. The normalized crystallinty of iPP and the PEOc component in the iPP/PEOc (80/20) blend was calculated based on Eq. (1), where ΔH_f^o for 100% crystalline polypropylene and polyethylene crystals is 209 [1] and 290 J/g [6], respectively. The total crystallinity of the iPP/PEOc (80/20) blend can be obtained according to Eq. (2):

$$X_c^t = 0.8X_c^{iPP} + 0.2X_c^{PEOc} \quad (2)$$

The results show that the crystallinity of the iPP component increases with the decrease of cooling rate (Table 4), which are

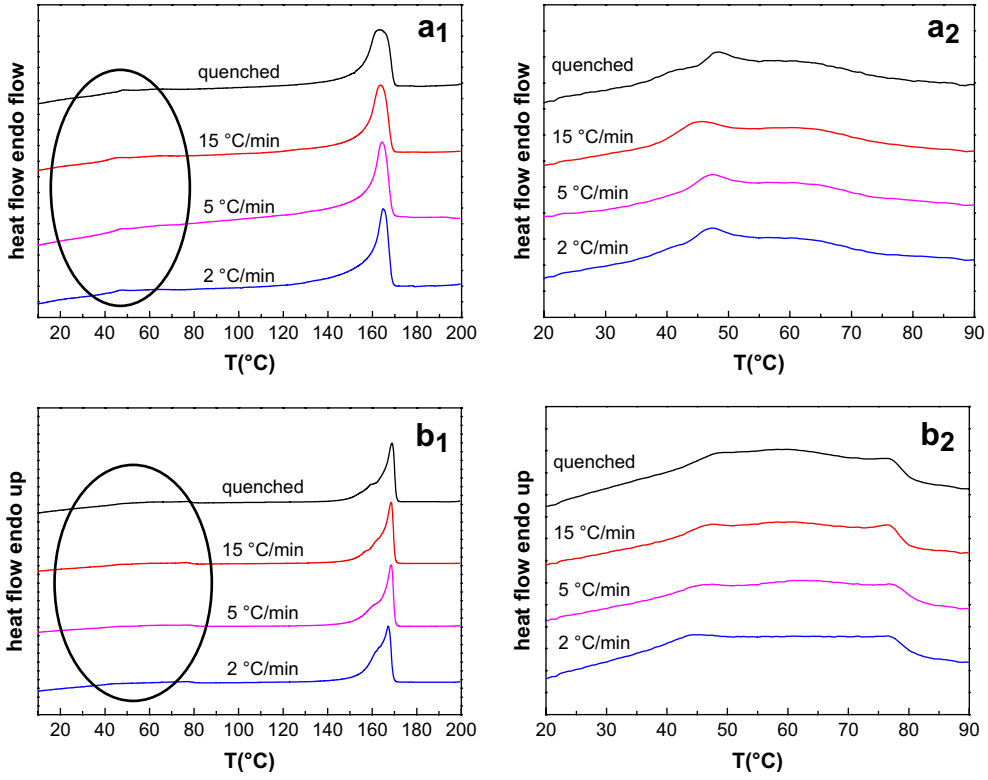

Fig. 5. DSC heating scans (10 °C/min) for undeformed regions (a_1 and a_2) and deformed regions (b_1 and b_2) of the iPP/PEOc (80/20) blend prepared at various cooling rates. The melting behavior of the PEOc component indicated by ellipses is amplified in Fig. 5a_2 and b_2, respectively.

Table 4
Melting behavior of undeformed regions of the iPP/PEOc (80/20) blend prepared at different cooling rates

Cooling rate (°C/min)		Quenched	15	5	2
Related to the PEOc component	T_{m1} (°C)	48.5	45.6	47.4	47.5
	T_{m2} (°C)	60.5	60.6	60.7	60.5
	ΔH (J/g)	7.0	6.9	6.2	6.5
	X_c^{PEOc}	12.1	11.9	10.7	11.2
Related to the iPP component	Onset (°C)	154.9	156.2	158.0	158.9
	T_m (°C)	163.3	163.3	164.4	164.6
	ΔH (J/g)	75.9	78.0	83.6	84.0
	X_c^{iPP}	45.4	46.7	50.0	50.2
	X_c^t	38.7	39.7	42.1	42.4

Table 5
Melting behavior of deformed regions of the iPP/PEOc (80/20) blend prepared at different cooling rates

Cooling rate (°C/min)		Quenched	15	5	2
Related to the PEOc component	T_{m1} (°C)	49.3	47.8	47.4	45.4
	T_{m2} (°C)	59.8	61.0	61.1	61.1
	T_{m3} (°C)	76.1	76.7	76.8	76.5
	ΔH (J/g)	19.2	15.4	14.5	15.4
Related to the iPP component	Onset (°C)	163.7	163.2	163.4	161.4
	T_{m1} (°C)	–	157.7	–	161.6
	T_{m2} (°C)	159.7	162.6	161.8	163.3
	T_{m3} (°C)	168.8	168.5	168.5	167.2
	ΔH (J/g)	80.8	80.0	83.3	85.6

comparative with those of pure iPP (Table 2). The crystallinity of the PEOc component is very low, nearly independent of the crystallization conditions. The total crystallinty of the iPP/PEOc (80/20) blend increases as the cooling rates decrease, which is responsible for its gradual depression of elongation at break and break strength.

The melting behavior of the deformed iPP/PEOc (80/20) blend (Fig. 5b_1 and b_2 and Table 5) was compared with that of undeformed region (Fig. 5a_1 and a_2 and Table 4). There are dual or multiple melting peaks for the iPP component of the deformed regions, and the higher one moves to higher temperature in comparison with those of the undeformed regions, while the lower ones appear as shoulder, the origin of which will be discussed later on. It is concluded that the original crystalline structure governs the mechanical properties, and the extensional deformation exerts significant influence on the final crystalline structure.

3.4. Influence of extensional deformation on crystallization behavior

3.4.1. WAXD characterization on structural deformation

X-ray diffraction is a powerful tool to characterize semi-crystalline polymers. First of all, 2D WAXD patterns were measured for the undeformed iPP specimens prepared at different cooling rates (Fig. 6a_1), which display diffraction rings. The circularly averaged integrated curves converted from the 2D WAXD patterns are shown in Fig. 6a_2, in which the diffraction peaks of $2\theta = 14.0°$, 16.8°, 18.6°, 21.2°, 21.9° are assigned to the crystal planes (110), (040), (130), (111), ($\bar{1}31$) of iPP α modification, respectively [23,31,34,40,41]. These diffraction patterns gradually become sharpened as the cooling rate decreases (from bottom to top), indicating the formation of crystallites with high lateral order or larger lateral size. Accordingly, the POM images show that the slower cooling rate is propitious for the formation of crystals with larger size and higher perfection. After tensile deformation (Fig. 6b_1), the crystalline rings are changed into arcs or even spots, meaning that the iPP chains were oriented preferentially to the tensile direction under stretching. It is further found in Fig. 6b_2 that after deformation, α crystals are distorted and the diffraction peaks turn to be irregular and much broader, indicating the decrease of crystallite size. The above WAXD results for the iPP samples indicate that under extension, the iPP crystals tend to dissociate into small crystallites, causing the broadening of diffraction peaks.

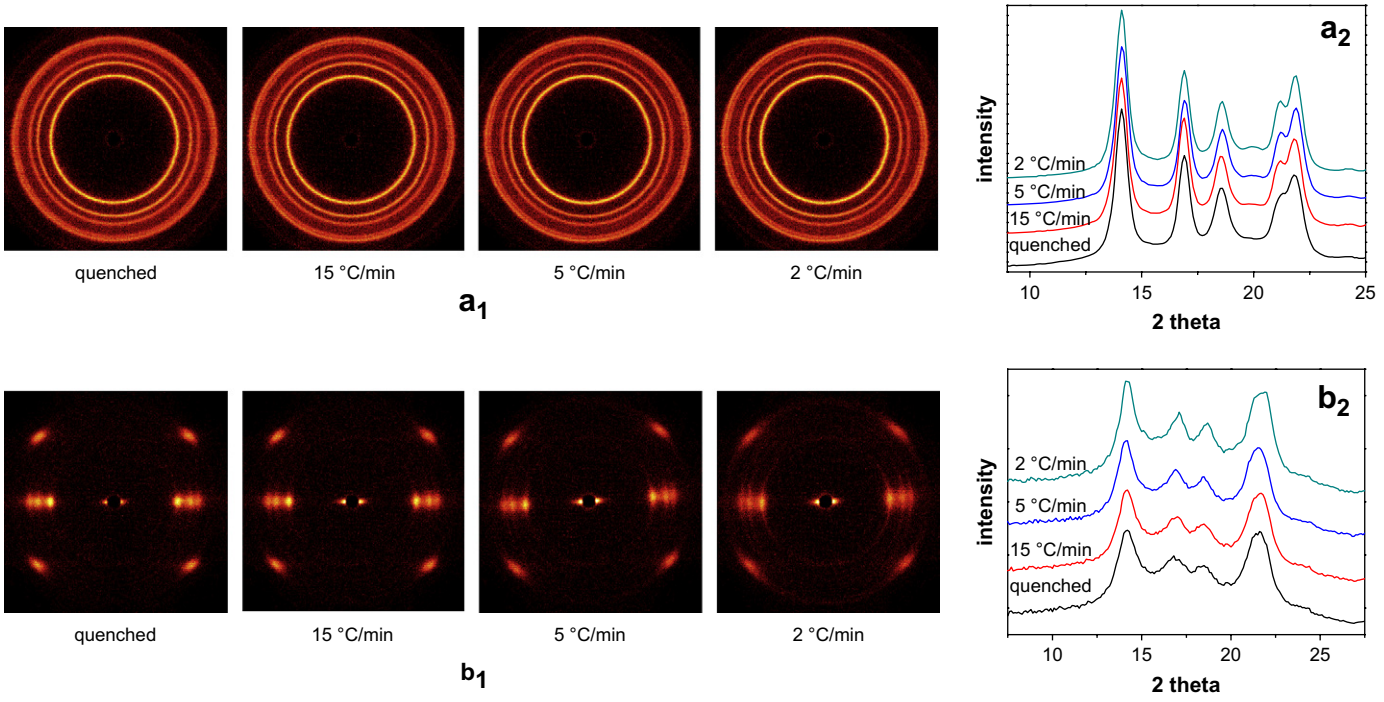

Fig. 6. 2D WAXD patterns of undeformed regions (a_1) and deformed regions (b_1) of the iPP specimens prepared at various cooling rates. The corresponding intensity curves of undeformed regions and deformed regions are also plotted in a_2 and b_2, respectively. The X-ray incident beam was perpendicular to the stretching direction (the meridian direction).

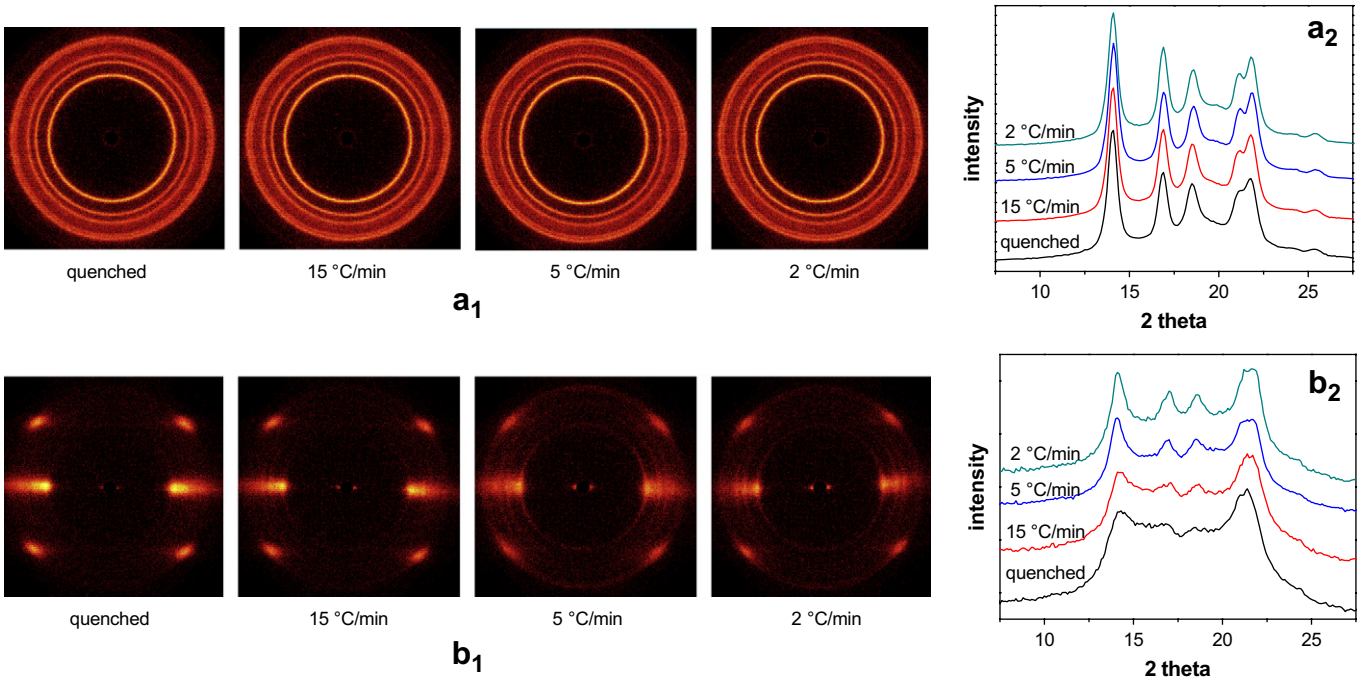

Fig. 7. 2D WAXD patterns of undeformed regions (a_1) and deformed regions (b_1) of the iPP/PEOc (80/20) blend specimens prepared at various cooling rates. The corresponding intensity curves of undeformed regions and deformed regions are also plotted in a_2 and b_2, respectively. The X-ray incident beam was perpendicular to the stretching direction (the meridian direction).

Similar to the WAXD results of pure iPP, the α crystals of the iPP component in the iPP/PEOc (80/20) blend gradually get more perfect as the cooling rate decreases (Fig. 7a_1 and a_2), whereas the diffuse amorphous halo is more obvious, for the addition of PEOc component can decrease the total crystallinity of the blend. After stretching, the diffraction spots emerge (Fig. 7b_1) and the changing of diffraction profiles (Fig. 7b_2) becomes much more prominent than those of pure iPP, implying that large deformation did occur for the iPP component in the blend, so that the crystalline lattice turns to be broadened. It is speculated that the large deformation of the iPP

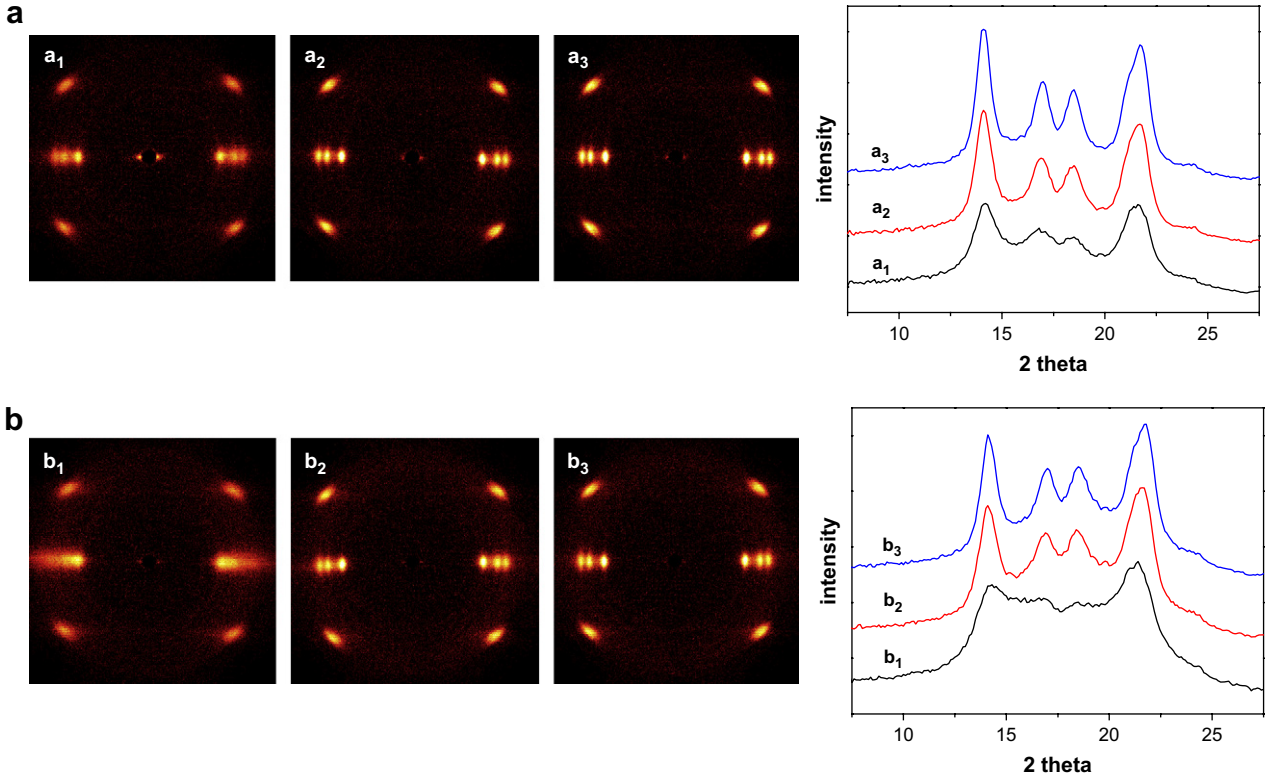

Fig. 8. 2D WAXD patterns of deformed regions of quenched iPP (a) and the iPP/PEOc (80/20) blend (b) specimens obtained at room temperature. The subscripts stand for different heat treatment: 1, no treatment; 2, heating from room temperature to 160 °C at 10 °C/min; 3, heating from room temperature to 160 °C at 10 °C/min and then annealing at 160 °C for 30 min. The corresponding intensity curves are also plotted.

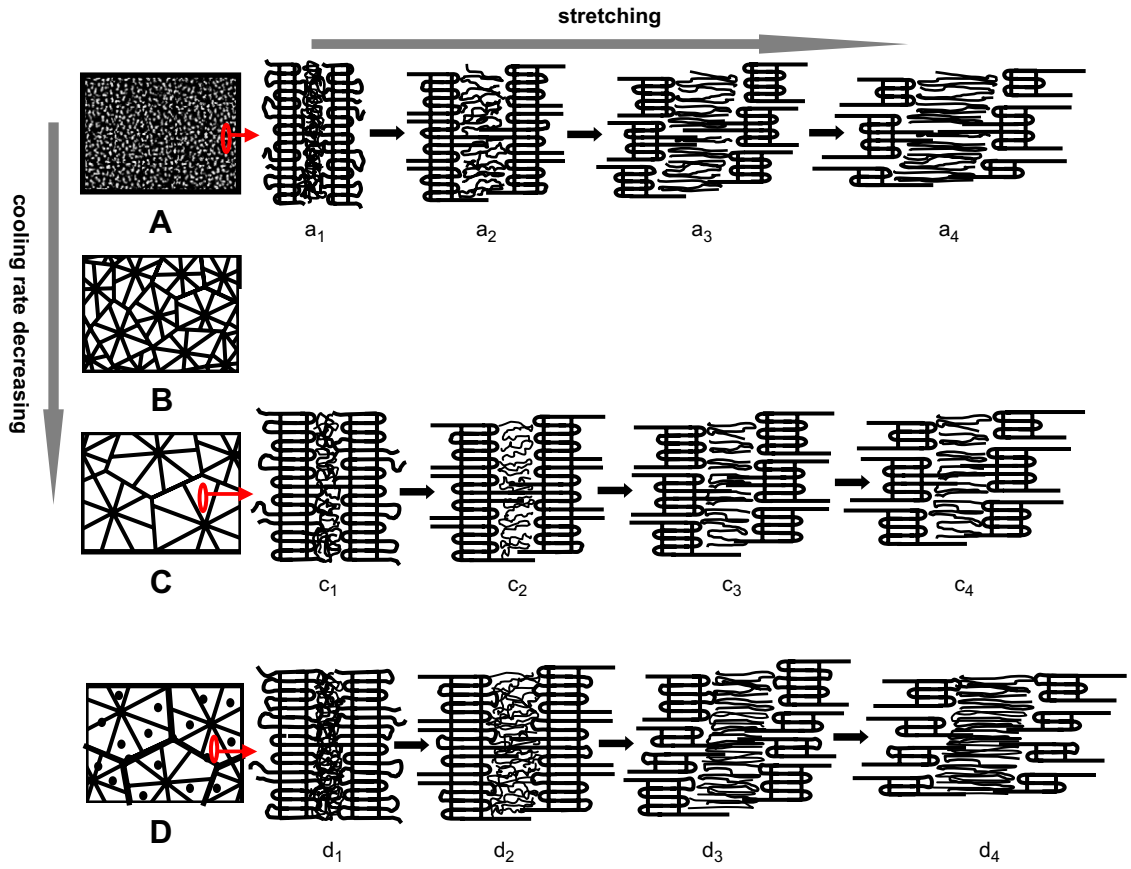

Fig. 9. Schematic illustrations of crystalline morphology of iPP (A, B and C) and the iPP/PEOc blend (D) samples prepared at different cooling rates and structural development under stretching. Only the lamellae in radial direction were taken as example. The cooling rate decreases from A to C. The iPP/PEOc (80/20) blend prepared at a slower cooling rate was selected for comparison with pure iPP correspondingly, and the dark points and diffuse boundaries in D represent the PEOc domains. The amorphous layer containing iPP and PEOc from d_1 to d_4 exists between the lamellar stack regions.

component is due to the interaction between iPP and the entangled PEOc molecules in the blend during the extension process.

After the extension of iPP (Fig. 6b_2) and the iPP/PEOc blend specimens (Fig. 7b_2), the broad and diffuse halo can be observed, which is related to the increase of oriented noncrystalline phase. In a previous report [34], similar noncrystalline phase was observed during stretching, called amorphous phase and smectic form. In order to clarify this issue, the deformed regions of quenched iPP and the iPP/PEOc (80/20) blend specimens were chosen to undergo different heat treatments (Fig. 8). After the samples underwent the heating runs at 10 °C/min from room temperature to 160 °C, the brightness of the diffraction spots and the intensity of the diffraction peaks (Fig. 8a_2 and b_2) increase compared with those of untreated specimens (Fig. 8a_1 and b_1), indicating that the crystallinity increases after the heat treatment. As the specimens underwent a further annealing treatment at 160 °C for 30 min (Fig. 8a_3 and b_3), the crystallinity of iPP and the iPP/PEOc blend continuously increases. The explanation for the crystallization variation is given as follows. The crystalline structure was partially destroyed after the tensile deformation, however, the oriented noncrystalline iPP molecular chains were easily reorganized into α modification under the postheating process, thus resulting in the increase of crystallinity. The WAXD results are in good accordance with DSC data, which have displayed that the melting enthalpy of deformed region is higher than that of undeformed region for both pure iPP and the iPP/PEOc blend, as revealed by the comparison of Tables 3 and 2, or Tables 5 and 4. It is claimed here that it is not proper to calculate the crystallinity of deformed regions with the melting enthalpy.

3.4.2. *Multiple melting phenomena*

Due to the influence of extensional deformation on the crystallization, the melting behavior of deformed region shows big difference compared with that of undeformed region for both iPP (Fig. 4) and the iPP/PEOc blend (Fig. 5). Figs. 3a and 4b show that the iPP sample undergoing crystallization at the cooling rate of 2 °C/min has the smallest elongation at break and only a single melting peak after stretched, while all the other samples have longer elongation at break and dual melting peaks, indicating that a proper elongation is propitious for the appearance of the dual or multiple melting peaks of iPP for the deformed regions. The occurrence of dual or multiple melting peaks is associated with a certain extent of structural deformation of the sample. In addition, it is worthwhile to note that the lower shoulder melting peaks of the deformed regions of the iPP/PEOc (80/20) blend (Fig. 5b_1) are not so obvious as those of pure iPP (Fig. 4b). In specific, the longer elongation and the consequent larger extent of distortion lead to the weaker shoulder melting peaks. Thus, it sounds reasonable to deduce that the larger distortion or dissociation or unfolding results in less remains of the original crystals during tensile deformation. Given longer time annealing or slower heating, the defective crystalline structure could be reorganized into crystals of higher perfection that could melt at higher temperature. The less prominent shoulder peaks of the iPP component in the iPP/PEOc blend might be due to the fact that the PEOc component lying among or between the iPP spherulites possesses more mobility to respond to the applied tensile deformation, and even promotes more deformation of the iPP crystals in the blend than in pure iPP.

The higher melting peak of the deformed region, no matter for iPP or the iPP component in the iPP/PEOc (80/20) blend, is higher than that of the corresponding undeformed region. It is generally recognized that the macromolecular chains orient and align preferentially to the tensile direction during stretching, and rearrange into crystals of higher perfection during the postheating process. Therefore, the higher melting peak is susceptible to the heating procedure, as well as the tensile deformation.

3.5. Deformation mechanism of iPP and the iPP/PEOc blend under extension

Based on the above discussion, schematic illustrations have been proposed for the deformation mechanism of both pure iPP (Fig. 9(A, B and C)) and the iPP/PEOc blend (Fig. 9D).

The sizes of the iPP crystals increase with the decrease of cooling rate (from A to C). Crystals formed at a higher cooling rate (Fig. 9A) are composed of thinner lamellae (Fig. 9a_1), thus the less perfect crystals have higher ability to respond to extensional deformation. In addition, more population of amorphous fraction connecting the crystallites adds to the interlamellar connections, resulting in larger elongation. As the imposed stretching proceeds, the dislocation, tilting and sliding of lamellae may occur under the extensional shear, and the molecules in the amorphous state gradually orient along the tensile direction (Fig. 9a_2). As the stretching is further imposed, the dissociation of lamellae and slipping of chains may occur (Fig. 9a_3), which result in the division of crystallites and disordering of the crystalline lattice. Given further extension (Fig. 9a_4), the dissociation of lamellae will be more prominent, and unfolding of molecular chains may occur, or even microfibrillation and cavitation. During the stretching, the molecules in the amorphous state are highly oriented in the tensile direction. In comparison, for samples prepared at slower cooling rate, larger spherulites are formed (Fig. 9C), comprising of thicker lamellae with higher perfection and stability (Fig. 9c_1). When stretched, it is difficult for the thicker lamellae to rearrange themselves to respond to tensile deformation, and the connections are weaker, so that the samples are fractured with shorter elongation. As the stretching is gradually applied, the chains are oriented preferentially in the tensile direction and the dislocation, tilting and sliding of lamellae may also occur (Fig. 9c_2). When the sample is further stretched, the dissociation and slipping within lamellae may also take place (Fig. 9c_3) and even unfolding of molecular chains (Fig. 9c_4). There is no doubt that the extensional deformation of the original crystalline structure is much obvious for the samples prepared at a higher cooling rate.

With the addition of PEOc component in the blend, the elastomeric phase will on one hand depress the perfection of the iPP crystals and on the other hand, enhance the connections of the iPP crystals, both of which are propitious to the extensional deformation. When stretched, both the iPP and the PEOc molecules will orient preferentially to the tensile direction, and much more structural change will happen than that of pure iPP. The structural development is established in Fig. 9 (from d_1 to d_4) for the iPP/PEOc blend prepared at a slower cooling rate. The dark points and diffuse boundaries in Fig. 9D represent the PEOc domains trapped in the iPP spherulites and rejected at boundaries, respectively. There may be some kind of interactions between the iPP and PEOc molecules during the extension, so it is conceivable that there must be more structural changes for the original iPP lamellae and even the amorphous regions. It is illustrated that more structural destruction, such as lamellae dissociation and unfolding of molecular chains could occur for the iPP component in the iPP/PEOc blend than for pure iPP. It should be pointed out that in Fig. 9, only the lamellae along radial direction were selected to show the structural development.

4. Conclusions

The uniaxially extensional deformation of pure iPP and the iPP/PEOc blend has been investigated considering the interaction between extensional deformation and crystallization behavior. The main conclusions are drawn here.

(1) The cooling rates dominate the crystalline structure and the consequent mechanical properties of both pure iPP and the iPP/PEOc blend.
(2) The PEOc component is believed to exist at interspherulitic regions or between lamellar stack regions, thus enhancing the crystalline connections and facilitating the elongation under extension.
(3) Orientation and destruction of partial crystalline structure were found under extensional deformation, and the oriented molecular chains can easily be reorganized into crystals of higher perfection during postheating procedure.

Acknowledgement

Financial supports from NSFC (20490220 and 50773087) are gratefully acknowledged. Y.Y. Pang thanks Prof. Z.G. Wang and Prof. S.K. Yan for helpful discussion.

References

[1] McNally T, McShane P, Nally GM, Murphy WR, Cook M, Miller A. Polymer 2002;43:3785–93.
[2] Da Silva ALN, Rocha MCG, Coutinho FMB, Bretas R, Scuracchio C. Polym Test 2000;19:363–71.
[3] Da Silva ALN, Rocha MCG, Coutinho FMB, Bretas R, Scuracchio C. J Appl Polym Sci 2000;75:692–704.
[4] Kontopoulou M, Wang W, Gopakumar TG, Cheung C. Polymer 2003;44:7495–504.
[5] Da Silva ALN, Tavares MIB, Politano DP, Coutinho FMB, Rocha MCG. J Appl Polym Sci 1997;66:2005–14.
[6] Bensason S, Minick J, Moet A, Chum S, Hiltner A, Baer E. J Polym Sci Part B Polym Phys 1996;34:1301–15.
[7] Bensason S, Nazarenko S, Chum S, Hiltner A, Baer E. Polymer 1997;38:3913–9.
[8] Prieto Ó, Pereña JM, Benavente R, Cerrada ML, Pérez E. Macromol Chem Phys 2002;203:1844–51.
[9] Premphet K, Paecharoenchai W. J Appl Polym Sci 2002;85:2412–8.
[10] Yang JH, Zhang Y, Zhang YX. Polymer 2003;44:5047–52.
[11] Pang YY, Dong X, Zhao Y, Han CC, Wang DJ. Polymer 2007;48:6395–403.
[12] Du J, Niu H, Dong JY, Dong X, Wang DJ, He AH, et al. Macromolecules 2008;41:1421–9.
[13] Samules RJ. Structured polymer properties: the identification, interpretation, and application of crystalline polymer structure. New York: John Wiley and Sons; 1974. p. 161–211.
[14] Peterlin A. J Mater Sci 1971;6:490–508.
[15] McConkey BH, Darlington MW, Saunders DW, Cannon CG. J Mater Sci 1971;6:572–81.
[16] Crist B, Fisher CJ, Howard PR. Macromolecules 1989;22:1709–18.
[17] Kennedy MA, Peacock AJ, Mandelkern L. Macromolecules 1994;27:5297–310.
[18] Kennedy MA, Peacock AJ, Failla MD, Lucas JC, Mandelkern L. Macromolecules 1995;28:1407–21.
[19] Liang S, Wang K, Yong H, Zhang Q, Du RN, Fu Q. Polymer 2006;47:7115–22.
[20] Na B, Wang K, Zhang Q, Du RN, Fu Q. Polymer 2005;46:3190–8.
[21] Men YF, Rieger J, Lindner P, Enderle HF, Lilge D, Kristen MO, et al. J Phys Chem B 2005;109:16650–7.
[22] Men YF, Rieger J, Homeyer J. Macromolecules 2004;37:9481–8.
[23] Lezak E, Bartczak Z, Galeski A. Macromolecules 2006;39:4811–9.
[24] Kazmierczak T, Galeski A, Argon AS. Polymer 2005;46:8926–36.
[25] Pluta M, Bartczak Z, Galeski A. Polymer 2000;41:2271–88.
[26] Bartczak Z, Krasnikova NP, Galeski A. J Appl Polym Sci 1996;62:167–79.
[27] Bartczak Z, Galeski A, Argon AS, Cohen RE. Polymer 1996;37:2113–23.
[28] Graham JT, Alamo RG, Mandelkern L. J Polym Sci Part B Polym Phys 1997;35:213–23.
[29] Mandelkern L, Smith FL, Failla M, Kennedy MA, Peacock AJ. J Polym Sci Part B Polym Phys 1993;31:491–3.
[30] Brooks NW, Ghazali M, Duckett RA, Unwin AP, Ward IM. Polymer 1999;40:821–5.
[31] Zheng Q, Shangguan YG, Yan SK, Song YH, Peng M, Zhang QB. Polymer 2005;46:3163–74.

[32] Nitta KH, Shin YW, Hashiguchi H, Tanimoto S, Terano M. Polymer 2005;46:965–75.
[33] Yamaguchi M, Miyata H, Nitta KH. J Polym Sci Part B Polym Phys 1997;35:953–61.
[34] Bedia EL, Murakami S, Senoo K, Kohjiya S. Polymer 2002;43:749–55.
[35] Kohjiya S, Tosaka M, Furutani M, Ikeda Y, Toki S, Hsiao BS. Polymer 2007;48:3801–8.
[36] Tosaka M, Senoo K, Kohjiya S, Ikeda Y. J Appl Phys 2007;101:084909 [1–8].
[37] Martins CI, Cakmak M. Polymer 2007;48:2109–23.
[38] Bensason S, Nazarenko S, Chum S, Hiltner A, Baer E. Polymer 1997;38:3513–20.
[39] Eckersley ST, Chaput AB. J Appl Polym Sci 2001;80:2545–57.
[40] Thomann R, Wang C, Kressler J, Mülhaupt R. Macromolecules 1996;29:8425–34.
[41] Thomann R, Semke H, Maier RD, Thomann Y, Scherble J, Mülhaupt R, et al. Polymer 2001;42:4597–603.